RSC Advances

ROYAL SOCIETY OF CHEMISTRY

www.rsc.org/advances

Silver nanoparticles prepared by gamma irradiation across metal organic framework templates

Li He, [a] **, Ludovic F. Dumée,* [a,b] *Dan Liu,* [a] *Leonora Velleman,* [a] *Fenghua She,* [a] *Connie Banos,* [c] *Justin B. Davies,* [c] *Lingxue Kong* [a]

[a] Institute for Frontier Materials, Deakin University, Pigdons Road, Geelong, Victoria, 3216, AUSTRALIA,

[b] Institute for Sustainability and Innovation, Victoria University, Hoppers Lane, Victoria, 3030 AUSTRALIA,

[c] Australian Nuclear Science and Technology Organisation, New Illawarra Road, Lucas Heights, New South Wales, 2234, AUSTRALIA

Corresponding author:

Li He

Doctor, Institute for Frontier Materials

Deakin University, Pigdons Road, Geelong

Victoria, 3216, AUSTRALIA

Email: li.he@deakin.research.edu.au

KEYWORDS: hybrid metal organic framework · surface catalytic materials · gamma irradiation · metal nanoparticle synthesis

ABSTRACT: In this study, we demonstrate for the first time the successful fabrication of well-dispersed ultrafine silver nanoparticles inside metal organic frameworks through a single step gamma irradiation at room temperature. HKUST-1 crystals are soaked in silver nitrate aqueous solution and irradiated with a Cobalt 60 source across a range of irradiation doses to synthesize highly uniformly distributed silver nano-particles. The average size of the silver nanoparticles across the Ag@HKUST-1 materials is found to vary between 1.4 and 3 nm for dose exposures between 1 and 200 kGy, respectively. The Ag@HKUST-1 hybrid crystals exhibit strong surface plasmon resonance and are highly durable and efficient catalytic materials for the reduction of 4-nitrophenol to 4-aminophenol (up to 14.46 x 10^{-3} s^{-1} for 1 kGy Ag@HKUST-1). The crystals can be easily recycled for at least five successive cycles of reaction with a conversion efficiency higher than 99.9%. The gamma irradiation is demonstrated to be an effective and environmental friendly process for the synthesis of nano-particles across confined metal organic frameworks at room temperature with potential applications in environmental science.

1. Introduction

Ultrafine metal nanoparticles (NPs) exhibit unique surface properties due to their enhanced plasmonic properties generated from the coupling of electromagnetic radiation wavelengths far larger than their physical size.[1] The high surface to volume ratio and the spatial confinement of electrons, phonons and electric fields at the interface between the NPs and their surrounding environment make them highly attractive materials with typically higher surface energy than bulk metal due to larger di-electric constant at the nano-scale.[2] Nano-structured materials based on metal NP assemblies are promising for photography, catalysis, biological labelling, photonics, opto-electronics and low concentration molecular sensing by Surface Enhanced Raman Scattering (SERS).[2-4] However, one of the major limitations in the synthesis and handling of ultrafine metal NPs relies in their unstable colloidal behaviour leading to both aggregation and coalescence under thermo-mechanical stress.[5] Advanced routes to synthesize ordered and yet stable arrays of NPs are therefore required to process materials exhibiting long term plasmonic properties.[1] Silver (Ag) NPs have been particularly studied due to their natural antimicrobial properties that can be explored for new disinfection routes in environmental engineering.[6] However the high surface energy, high reactivity and strong cohesion of the ultrafine Ag NPs all contribute to their easy aggregation.[7]

A promising approach to preventing such aggregation is to control both the size and shape of the silver NPs by discretely growing them across nano-porous cages. The confinement of the growth within nano-spaces as a hard template[5, 8-10] or the introduction of a soft protective material around the pre-formed NPs[11-14] are the two most established methods to alleviate aggregation. The immobilization of the NPs within a solid support matrix or ligand such as carbon,[11, 12] silica[13] and metal oxides,[14] may allow for the formation of macro-assemblies of NPs

but can reduce the reactivity of the NPs due to specific site coordination. This synthesis technique may not provide long range three-dimensional structures and will reduce contacts between the NPs and their environment.[4] However, the controlled growth of NPs across highly organized arrays of micro- or meso-porous materials such as zeolite[8, 9] and Metal Organic Frameworks (MOFs)[5, 10] as a hard template would allow for the formation of an internal confined metal NPs with diameters proportional to their template size and likely up to tens of angstroms.[4]

The architectures of MOF materials provide well-defined interconnected pore channels, large internal surface areas and tuneable surface chemistry to prevent the aggregation of NPs. [15-18] Different MOF architectures including ZIF-8,[19, 20] MOF-5,[4, 21] or MIL-101[22, 23] have been used as host templates for the incorporation and growth of metal or metal oxide nano-clusters and NPs, such as gold (Au), Ag, palladium (Pd) and ruthenium (Ru). These materials were synthesized by various techniques including chemical vapour deposition,[21] liquid/incipient wetness impregnation,[24] solid grinding in contact with reducing agents,[25] heat gradients[20] and UV irradiation.[4] Pd, Au and copper (Cu) NPs with size distributions between 5-20 nm were obtained across the nano-scale pores of MOF-5 single crystals using organo-metallic chemical vapour deposition (OMCVD).[21] Ultrafine 1.5 nm diameter Au NPs were incorporated across MOFs by solid grinding of Au particles,[25] while UV irradiation has been used to directly reduce micron-sized Ag NPs inside a pre-formed MOF-5 matrix.[4] However, these synthesis techniques present drawbacks, including low penetration depth and potentially damaging the MOF materials, while also requiring high pressure and temperature and producing by-product during reduction.[26] Novel non-destructive and environmentally friendly techniques to produce metal-MOFs particles are still required.

Recent work on radiation chemistry suggests that gamma irradiation is effective at reducing metal ions into metal particles in genuinely mild chemical conditions.[26] Radiation chemistry is a simple, cost-effective and efficient strategy to uniformly induce chemical reactions across thick layers of materials due to great penetrability of gamma radiation through organic matters without noticeable decay of the organic matrix.[27, 28] Irradiation was also demonstrated to be an effective method to increase the kinetics of metal ion reduction at ambient temperature without excessive reducing agent thus leading to a more environmentally friendly process to generate metal NPs.[26]

Here, HKUST-1 crystals,[29-31] which consist of Cu^{2+} coordinated to trimesic acid (TMA) linkers, forming a highly inter-connected 3D sub-nanometre network, have been chosen as a hard template for ultrafine Ag NPs synthesis. The high surface area of the material (692 m^2/g), high thermal stability (up to 240°C), narrow nano-scale scale cage size distribution (18.6 Å), as well as well-defined interconnecting channels (9 Å by 9 Å pore) and excellent water stability make HKUST-1 an ideal hard template for producing mono-dispersed ultra-fine Ag NPs.[30] In this paper, we report for the first time a single step technique to produce metal NPs in a highly controlled fashion with extremely narrow size distributions across MOFs crystals by gamma irradiation. The properties and crystalline structure of the MOF and Ag NPs synthesized across the cages will be assessed and discussed in addition to their catalytic properties. This presents a facile, high yield and up-scalable route, due to the high penetration depth of gamma radiation across polymeric matters, to reduce silver ions across HKUST-1 crystals at room temperature while preventing particle aggregation.

2. Experimental

2.1 Preparation of HKUST-1 crystals

HKUST-1 crystals were prepared following a method described previously.[29] In a typical synthesis procedure, 4.55 g of $Cu(NO_3)_2 \cdot 3H_2O$ were dissolved in 60 ml of deionized water while 2.10 g of TMA was separately dissolved in 60 mL of ethanol. The TMA solution was then added into the $Cu(NO_3)_2 \cdot 3H_2O$ solution and kept under vigorous stirring for 10 min prior to being poured in a 200 mL Teflon liner. The Teflon liner was then placed in a steel autoclave and heated at 100 °C for 18 h. The after growth product was thoroughly rinsed with ethanol by vacuum filtration and dried at 150 °C under vacuum (10^{-5} Torr) for 24 h.

2.2 Reduction process of silver ions across HKUST-1 crystals

The freshly synthesized HKUST-1 crystals were activated under low vacuum at 100 °C for 12 h, and then pure solvent free HKUST-1 template (500 mg) was placed in a 4 ml glass vial. A 0.50 M $AgNO_3$ solution was prepared by dissolving 0.25 g of $AgNO_3$ in 500 µL of Milli-Q water and then diluting with 3 mL of ethanol. The Ag salt solution was then transferred into a glass vial containing the degassed HKUST-1 crystals to generate a slurry. The reaction vessel was backfilled with N_2, hand-shaken for 1 min to ensure thorough mixing, and placed into a cobalt-60 gamma irradiation facility at the Australian Nuclear Science and Technology Organisation (ANSTO). Irradiations were carried out at a dose rate of 3.3 kGy/h, measured using calibrated ceric-cerous dosimeters,[32] for a range of irradiation doses between 1 and 200 kGy. After irradiation, the Ag@ HKUST-1 crystals were immediately rinsed with ethanol to remove remaining excessive metal salts and the samples were then degased at 150 °C for 16 h in a vacuum oven.

2.3 Morphology and crystallinity characterisation techniques

Scanning Electron Micrographs (SEM) were acquired on a Supra SEM 55VP field emission microscope with an Energy-dispersive X-ray spectroscopy (EDX) detector (Oxford X-Max 20 Silicon Drift detector, UK). All samples were carbon coated prior to imaging and an accelerating voltage of 5 keV and 20 keV were respectively used for imaging or elemental mapping at a fixed 10 mm working distance. High resolution Transmission Electron Micrographs (TEMs) were captured on a JEOL JEM-2100 at 200 keV. The NP size distributions were obtained on at least 100 NPs and the resultant data were plotted by class of 0.2 nm in histograms. Fourier transform infrared (FTIR) spectra were obtained by mixing the powders with potassium bromide (KBr) to form homogenous disks. Typically, 1 mg of Ag@HKUST-1 powder was mixed with 200 mg of KBr and compacted into disks. The spectra were recorded in the range of 600 - 4,000 cm^{-1} at a resolution of 4 cm^{-1} with a Bruker Vetex-70 FTIR spectrometer. Pure HKUST-1 crystals were measured on the Powder Diffraction beamline (M5863) at the Australian Synchrotron using a wavelength λ = 0.774346 Å to evaluate the crystalline structure of the HKUST-1 crystals by structure refinement analysis. The samples were ground into fine powders and then sealed into a 0.5 mm diameter Thin-Walled capillary quartz tubes prior to being rotated at 100 rpm for 5 min. All the structure refinements were performed using the Rietveld method with GSAS software. Powder X-ray diffraction (PXRD) of the Ag@HKUST-1 powder samples were also recorded with a PANalytical's X'Pert Power X-ray Diffraction (40 keV, 30 mA) with Cu Kα radiation (λ = 1.548 Å) in the range of 2θ = 5 - 60° by steps of 0.05° and a scanning rate of 0.02° $mins^{-1}$. Raman spectra were obtained on a Renishaw inVia Raman microscope (Renishaw Gloucestershire, UK) at a laser wavelength of 514 nm. Acquisition parameters used for the spectral data collection included a 30 s exposure time at 1% nominal laser power and for 1

accumulation at a spectral resolution of 4 cm^{-1}. All spectra were taken with a microprobe apparatus consisting of a 20x objective to focus the incident light on a spot of ~ 1.9 μm^2. The specific surface area of the samples was determined by Brunauer–Emmett–Teller (BET) surface analysis across a pressure range of $p/p_o = 0.1 - 0.3$ at 77 K. Thermal Gravimetric Analysis (TGA) results were obtained using a STA 449 Jupiter Netzsch DSC/TGA in air from 150 °C to 700 °C and a heating temperature rate of 10 °C min^{-1}.

2.4 Catalytic reduction of 4-nitrophenol

The catalytic reduction of 4-nitrophenol (4-NP) by $NaBH_4$ was chosen as a model reaction to investigate the catalytic capacity of the Ag@HKUST-1 crystals. In a typical experiment, 14 ml deionised water and 750 µL 4-nitrophenol (3 mM) were mixed with 1mL of freshly prepared sodium borate ($NaBH_4$) (0.3 M). A solution volume of 3 ml was transferred into a quartz cuvette. 2 mg (± 0.005 mg) of powder samples were immediately added into the quartz cuvette. The *in situ* UV-Vis absorption profiles were recorded in Ocean optics USB2000 Miniature Fiber Optic Spectrometer with PX-2 Pulsed Xenon Light Source in the range of 250-550 nm to monitor the catalytic reaction and kinetics of degradation of the 4-nitrophenol by recording over time the intensity of the peak at 317 nm.

3. Results and discussion

The Ag@HKSUT-1 crystals were prepared by mixing HKUST-1 crystals with the Ag salt solution prior to exposure to a range of gamma radiation doses as depicted in **Figure 1a**. Gamma irradiation produces solvated electron which reacts very fast with nitrate ions taken in the form of silver nitrate. The reactive composed of both oxidative and reductive species that were generated from radiolysis of water reacts competitively with Ag^+ and NO^{3-} inside HKUST-1

crystals to produce Ag nanoparticles. The structure of the HKUST-1 was analysed by Powder Diffraction (PD) at the Australian Synchrotron and a Rietveld refinement factor of 4.41 was calculated, suggesting that the structure and morphology of the HKUST-1 are cubic unit cells with a highly inter-connected 3D sub-nanometre network (**Figure 1b**).[29-31] Based on the PD refinement, the synthesized HKUST-1 particles were found to present a cubic structure with lattice parameters a_0 of 26.37 Å and a volume of 18,343.8 $Å^3$. The simulated HKUST-1 crystalline structure was found to be a face-centred-cubic crystal containing large square-shape channels with pore dimensions of 9 by 9 Å. A view down the [111] direction of the cubic cell of HKUST-1 reveals a honeycomb arrangement of large hexagonal-shaped windows with an inner cage diameter of 18.6 Å. These confined cages at the intersection between a set of 3 orthogonal channels formed very adequate cavities for templating NPs growth by *in-situ* metal ion reduction. The synthesized HKUST-1 crystals were obtained as single blue-coloured crystalline octahedron shapes of a few microns in size (**Figure 1c**) with the colour being progressively turned to darker green upon exposure to gamma radiation (**Figure 1d**).

The morphology of the Ag@HKUST-1 crystals was investigated upon the series of irradiation doses and shown across the series of scanning electron microscopy (SEM) images in **Figure 2**. Albeit the visible colour change of the powders and crystals, the overall morphology of the HKUST-1 crystals, (~10 ±2 μm in diameter) remained the same as that of the pristine crystals even after irradiation dose of 100 kGy suggesting little, if no, damage to the materials. Interestingly at an irradiation of 200 kGy, dark areas appeared on the surface of the HKUST-1 crystals, indicating localized damage to the crystalline structure which was attributed to the de-coordination of the TMA ligands from the copper ions.[33, 34] Elemental distribution across the surface of the crystals was evaluated by EDX for the series of composite samples at different

doses and the elemental distributions of C, O, Cu and Ag are presented in **Figure 2f**. It can be clearly seen that, although the Cu background is strong across the entire surface, the crystals are covered with Ag. In addition, the relative intensity of the Ag signal is increases with the radiation dose suggesting an increase of the reduced Ag_0 metal with irradiation. Furthermore, the penetration depth of the electron beam at 20 keV can be expected to reach 200 nm to 2000 nm, suggesting that particles are indeed present deep across the structure.

This is confirmed by TEM analysis of the irradiated samples (**Figure 3** and **Figure 1S)**. As clearly seen from the images and histograms, the size and density of the reduced Ag NPs increase steadily with the radiation dose with a levelling off above 100kGy. The average diameter of Ag NPs increases from 1.4 to 3 nm between 1 and 100 kGy, respectively. The shape of the NPs is largely spherical although slightly elliptical particles are visible on the 200 kGy samples. The particle size distribution is also found to be very narrow with standard deviations smaller than 20% of the nominal average values. In addition, the particle density across the crystals increases with radiation dose. Thermal Gravimetric (TGA) analysis was therefore performed to evaluate the thermal stability of the crystals as well as the overall content in Ag. The TGA results (**Figure S3)** indicate that the pristine HKUST-1 crystals are extremely stable up to 300 ºC. A low but gradual weight loss of 4.94 wt% is found between 150ºC and 300ºC for the pristine sample which is attributed to the evaporation and loss of physisorbed and chemisorbed solvent molecules within pores or on the surface of the material.[35] The further weight loss above 300^{o}C corresponds to the progressive decomposition of the organic TMA ligand molecules which results in an overall loss of ~36.84 wt%. The dry residual weight of the pristine sample is ~41.78 wt% at 700ºC which corresponds to the formation of copper oxides from the freed copper ions present in the framework. A similar degradation pattern was observed for the gamma

irradiated samples and as expected from the Ag NPs presence, the final relative weights varied between 43.33 wt% and 50.22 wt% for the 1 and 200 kGy irradiated samples, respectively. This further confirms that the particle density increases with the irradiation dose.

In addition, the size of the Ag NPs visible on the TEMs is smaller than that of the HKUST-1 cage size (18.6 Å) up to 1 kGy of exposure. However, above 1 kGy of exposure, corresponding to an irradiation time of approximately 18 min at 3.5 kGy/h, the size of the particles exceeds that of the host cage, for example, by up to 40 % at 100 kGy. This discrepancy suggests potential Ag NPs decorating the outside of the HKLUST-1 particles or potential localized deformation of the MOF sub-structure and the formation of nano-strains across the material which could lead to an increased overall particle density and partial collapse of the crystals for the exposure of 200 kGy (**Figure 3**). This is consistent with the XRD results presented in **Figure 5** where no significant crystalline changes across the pristine and the hybrid crystals can be reported up to 200 kGy. This trend indicates that HKUST-1 materials are reasonable stable under gamma irradiation and that almost all Ag NPs are well intercalated within the sub nanoscale pores of HKUST-1. HKUST-1 crystals exhibit an appropriate surface Gibbs free energy and a suitable cage size to host relatively large Ag NPs. Furthermore, as observed from the XRD spectrum, the peak at 38° is attributed to the Ag (111) reflection, suggesting the formation of crystalline Ag sub-structure within the MOF hosts. The peaks of HKUST-1 after different irradiation doses became weaker than original HKUST-1 as the high concentration of silver NPs potentially affected original HKUST-1 peaks and led to a strong peak at 38°. The overall peak was found to be very weak and much broader at 200 kGy, which is attributed to the much larger distribution of Ag particles formed and potentially to the fact that the HKUST-1 original structure may have been heavily damaged at such a high radiation dose. Chemical degradation of organic and organo-metallic

materials was previously reported for HKUST-1 and was primarily related to hydrolysis mechanisms.[33, 34] A hydrolysis reaction of water molecules with Cu-O-C group induces the paddle wheel structural decomposition.[33]

FTIR spectroscopy was also used to confirm potential chemical degradation on the surface of the samples. While the FTIR patterns of the pristine HKUST-1 (**Figure S2**) match well that available in the literature[36] the asymmetric stretching vibrational of -(O-C-O)- groups around 1700 and 1500 cm^{-1} and symmetric stretching vibrational of -(O-C-O)- groups around 1500 and 1300 cm^{-1} that are characteristics of the TMA molecules, are clearly visible for all of the samples. FTIR spectra at 1452 cm^{-1} are due to a combination of benzene ring stretching while the bonds around 730 cm^{-1} are ascribed to the C-H vibration of the ligand molecules. The vibrational band corresponding directly to the ligand linked through the centred Cu ions is also visible on the IR absorption band at 491 cm^{-1} and no obvious differences were found between the irradiated samples and the pristine samples, which indicates that Ag@HKUST-1 crystals are chemically stable upon gamma irradiation. The chemical composition of the samples was found to be maintained upon gamma irradiation which demonstrates that the nature of the damages across the MOFs is more likely to be physical from localized deformations of the matrix upon particle growth rather than chemical from the degradation of the ligands. The nitrogen adsorption - desorption isotherms at 77 K (**Figure 6**) were used to calculate the specific surface area of Ag@HKUST-1 with different Ag NPs loading (**Figure S4**). The BET surface area and pore volume of the pristine non-irradiated HKUST-1 crystals are 739.86 m^2 g^{-1} and 0.12 cm^3 g^{-1}, respectively. As expected due to the increased presence of the Ag NPs, the BET surface area of the samples steadily decreasing from 650.62 m^2 g^{-1} to 588.34 m^2 g^{-1} upon irradiation between 1 and 100 kGy, respectively. This decrease in surface area after Ag NPs loading supports the

previous information on the particle dispersion across the crystals. It suggests that the MOFs cavities are occupied and that pores are potentially obstructed by the larger Ag NPs located at the entrance of the channels on the crystals surface. Furthermore, the surface area of the 200 kGy sample (436.34 m^2 g^{-1}) is nearly 50% lower than that of the pristine sample and 34% lower than the 100 kGy irradiated crystals. This sharp decrease also suggests localized degradation upon extreme gamma irradiation. The N_2 isotherm increases to the range of 0.8-1.0 P/Po due to HKUST-1 particles being accumulated and formed in the macropores between HKUST-1 particles.

In addition, the presence of larger Ag NPs is also shown on the surface of the crystals for the 10, 100 and 200 kGy irradiated samples. This indicates that some Ag^+ ions present in the bulk solution were also likely reduced outside of the host matrix and that their crystallization may have been preferentially seeded on the external surface of the crystals due to the presence of semi-coordinated copper ions acting as reducing catalysts.[5] The presence of larger particles at higher irradiation doses also suggests that some aggregation may have occurred, potentially upon drying of the powders after synthesis. This phenomenon was previously reported for Ag@MOF $[Ni(C_{10}H_{26}N_6)](ClO_4)_2$[37] by Redox-Active MOFs and Au@CPL-1[25] by solid grinding. Although no isolated Ag NPs were found in the solutions or in the vicinity of HKUST-1 crystals on the TEMs, it is possible that individual Ag NPs may have been washed away upon rinsing and washing of the samples due to their nano-scale size. The presence of larger Ag aggregates and higher density of Ag NPs at 200 kGy is however consistent with the overall trends which suggests that an optimum reduction for this system might fall between 1 and 10 kGy. This dose exposure would lead to perfectly fit particles without leading to structural damages to the host structure.

Furthermore, in order to evaluate the Ag NPs accessibility from the crystals surface, SERS experiments were performed on specific peaks related to the TMA ligands. As previously reported, the shape, size and density of metal NPs scattered across a surface will strongly affect the strength of the Raman signal enhancement which can potentially allow for the identification or detection of chemicals adsorbed on a surface even at very low concentration.[38] The largest enhancement factors were typically reported for large density, sub-100 nm particle arrays such as Ag and Au NPs.[38] A typical Raman absorption spectrum of HKUST-1 crystals is shown in **Figure S5**. The bands at 1610 and 1006 cm^{-1} dominate with C=C modes of the benzene ring while peaks at 826 and 740 cm^{-1} are associated with out-of-plane ring (C-H) bending vibrations and out-of-plane ring bending, respectively. [38, 39] In addition, doublets at 1550 and 1460 cm^{-1} are typically ascribed to the v_{asym} ($C\text{-}O_2$) and v_{sym} ($C\text{-}O_2$) units. Eventually, complex bands at 500 cm^{-1}, 275 cm^{-1} and 177 cm^{-1} indicate the presence of CuO_2.[36] Here, very strong enhancement factors can be observed on the irradiated HKUST-1 crystals which were significantly modulated by the relative amount of Ag NPs content as shown in **Figure 7**. The intensity of 200 kGy irradiated samples is 98 times greater than pure HKUST-1 crystals which shows a strong Raman enhancement at peak 1600 cm^{-1}. The magnitude of the spectra increases significantly with irradiation, which is consistent with a progressive increase of the Ag NPs density distribution. The permanent and significant increase in the magnitude of the Raman scattering peaks for the Cu related bonds also suggests strong interactions between the HKUST-1 crystals and the Ag NPs present across the HKUST-1 host. This is a very significant result since it also demonstrates that the hybrid HKUST-1 particles may be used for fine chemical sensing and that even low radiation doses may be sufficient to fabricate Raman active materials.

Finally, the catalytic properties of the hybrid HKUST-1 crystals were investigated through specific decomposition of 4-nitrophenol (4-NP) as a reference reaction. This largely non-biodegradable chemical is has been extensively used for pesticides and herbicides and typically leads to strong water pollution in agricultural intensive areas.[6] Furthermore, one of its derivatives, 4-AP, is a very popular non-hazardous chemical used in the formulation of drugs such as analgesic and antipyretic chemicals which have been used as photographic developer, corrosion inhibitor, anticorrosion lubricant, and in hair dying agents.[6] Therefore, it is highly desirable to develop more efficient, durable and eco-friendly catalytic systems to produce 4-AP by reducing 4-NP. For this reason, the reduction of 4-NP into 4-AP by $NaBH_4$ in the presence of noble metal nanoparticles as catalysts (such as Au, Ag and Pt) have been extensively studied.

Here, the catalytic reduction of 4-NP by $NaBH_4$ was chosen as a model reaction to investigate the catalytic capacity of the Ag@HKUST-1 particles. A comparative study of the Ag@HKUST-1 catalytic activity was performed as a function of different radiation doses. This reduction process may however not proceed with the presence of HKUST-1 crystals alone due to their lack of intrinsic catalytic activity (**Figure S6**). The reaction therefore requires the presence of Ag_0 as a catalyst to overcome the activation energy kinetic barrier of the reduction reaction of 4-NP.[40] Metal nano-catalysts, such as Ag NPs, may act as an electronic relay system to activate the 4-NP molecules prior to being regenerated upon full reduction in $NaBH_4$. **Figure 8** presents a representative UV-visible spectrum of the reduction of 4-NP by 100 kGy Ag@HKUST-1 crystals at room temperature over time. The absorption peak of 4-NP in presence of $NaBH_4$ at 400 nm decreased quickly after the addition of the 100 kGy Ag@HKUST-1 catalyst with the yellow-green colour turning into a colourless solution, representative of a complete degradation. In the reduction process, the concentration of $NaBH_4$ is much higher than that of 4-NP and can

therefore be considered as constant during the reduction reaction. The chemical reduction can be considered as a pseudo-first-order reaction based on the evaluation of the rate constant with regards to 4-NP only.[41] Hence, the reduction can be described as $ln(C_t/C_0) = -kt$, where k is the apparent first-order rate constant (s^{-1}), t is the reaction time, C_t is the concentration of 4-NP at time t and C_0 is the initial concentration of 4-NP. $ln(C_t/C_0)$ vs. time can be obtained based on the absorbance as the function of time, as shown in **Figure 8**. It shows a linear relationship between $ln(C_t/C_0)$ and reaction time t in the reduction catalysed by Ag@HKUST-1. The full reduction of 4-NP by $NaBH_4$ was completed within 300 s which gives a reaction rate constant k of 14.25 × 10^{-3} s^{-1} for the 100 kGy Ag@HKUST-1 catalyst, which is 250%, 216%, 130% and 280% higher than that of Ag NPs using stem extract of Breynia rhamnoides method,[42] magnetically separable alginate-based biohydrogels@Ag composite [6] and carbon nanofibers@Ag,[43] ZIF8@Ag,[41] respectively, but 12% lower than that of silica nanotubes@Ag.[40]

For comparison, the catalytic performance of the series of gamma irradiated samples were also investigated and the reduction reaction kinetics are summarized in **Table 1**. The results show excellent catalytic activities of all the Ag@HKUST-1 due to their high specific surface area (436 to 650 m^2/g) and the highly dispersed and individualized nature of the Ag NPs (1.4 to 3 nm). These surface properties allow for excellent contact between the particles and the 4-NP during the reaction. The 1 kGy Ag@HKUST-1 catalyst shows the best kinetic reduction rate of 14.46 x 10^{-3} s^{-1} which is 23% higher than 200 kGy Ag@HKUST-1. However, the apparent first-order rate constant k of 10 kGy Ag@HKUST-1 is slightly lower that of the 100 kGy Ag@HKUST-1 due to higher loading of Ag NPS across the HKUST-1. Therefore, in order to further investigate the catalytic property of AG@HKUST-1, the rate constants on a per gram basis of Ag NPs (K_{Ag}) were then calculated and presented in **Table 1**. The result shows that the

kinetic constant is inversely proportional to the diameter of the Ag NPs which highlights the role of the Ag NP size in enhancing the catalytic degradation performance.

Eventually, in order to evaluate the recyclability of the Ag@HKUST-1 catalysts, a series of successive cycles of catalytic reductions were carried out with the particles. As shown in **Figure 8**, the catalyst particles can be successfully recycled and reused for up to 5 subsequent cycles of reaction but still remain a conversion efficiency of higher than 99.9%, allowing for an efficient recycling of the Ag@HKUST-1 catalysts. After the first run, the rate constant decreases as the particles are not very stable in the presence of alkaline environment ($NaBH_4$ solution). The catalyst rate keeps almost constant after 1st cycle, SEM images of 100 kGy Ag@HKUST-1 crystals after 5 cycle (**Figure S7**) show that there is degradation happening during the reaction but the HKUST-1 crystals still keep their original octahedron shape and no big difference was shown in TEM images (**Figure S8**). No major differences were observed across the series of samples and all consecutive tests led to highly similar and reproducible results. A longer reaction time of 1200 s was, however, required to achieve the full reduction of 4-NP by $NaBH_4$ after the 5th cycle by using the same 100 kGy Ag@HKUST-1 crystals as catalysts. This translates into a kinetic reduction rate of 4.35×10^{-3} s^{-1} at that dose suggesting a decrease of approximately 65 % over the scope of the cycles. This result is significant since it demonstrates the potential of the Ag@HKUST-1 catalyst and the positive impact of the Ag NPs on the catalytic properties of the material in the reduction of 4-NP.

4. Conclusions

In summary, a novel approach to preparing highly catalytic Ag hybrid HKUST-1 crystals was demonstrated by in-situ gamma irradiation reduction of silver ions across a MOF host

template. HKUST-1 crystals exhibit well-defined channels and tuneable nano-scale cavities which were demonstrated to be flexible enough to allow for a degree of deformation upon particle growth. Ag NPs with very narrow and uniform particle size distributions, between 1.4 and 3 nm can be readily synthesized across and decorated on the surface of HKUST-1 crystals. The results indicate that Ag@HKUST-1 crystals have significantly improved enhancements factors for surface enhance Raman spectroscopy. They are highly stable in water based environment and can be promising candidates for low concentration chemical sensing. Furthermore, the Ag@HKUST-1 crystals exhibited a highly efficient catalytic activity for 4-NP reduction by $NaBH_4$. The 1 kGy Ag@HKUST-1 exhibited the highest catalytic activity with a kinetic reduction rate of up to 14.46×10^{-3} s^{-1}. Most remarkably limited diminution of the catalytic activity of the samples was detected after five consecutive cycles, demonstrating the excellent chemical stability and reusability of the crystals for catalysis applications and the potential of using MOF templating for metal NP growth.

Supporting Information

Supporting Information is available free of charge via the Internet at http://pubs.acs.org.

Acknowledgement

Dr. Li He has been supported by Deakin University through Alfred Deakin Fellowship while Dr. Ludovic Dumée was funded by the Cooperative Research Network (CRN) funding 2012/2. The project has also been support by the Australian Synchrotron under the beamtime M5863 with special thanks to Dr. Justin Kimpton and Dr. Qinfen Gu. The authors also acknowledge the AINSE grant (ALNGRA13064), Dr. Andrew Sullivan for advice with SEM imaging, Dr. Rosey Van Driel for advice with TEM imaging and Dr. Pimm Vongsvivut for help with Raman analysis.

References

1. E. C. Le Ru, E. Blackie, M. Meyer and P. G. Etchegoin, *The Journal of Physical Chemistry C*, 2007, 111, 13794-13803.
2. T. K. Sau, A. L. Rogach, F. Jäckel, T. A. Klar and J. Feldmann, *Advanced Materials*, 2010, 22, 1805-1825.
3. C. Burda, X. Chen, R. Narayanan and M. A. El-Sayed, *Chemical Reviews*, 2005, 105, 1025-1102.
4. R. Ameloot, M. B. J. Roeffaers, G. De Cremer, F. Vermoortele, J. Hofkens, B. F. Sels and D. E. De Vos, *Advanced Materials*, 2011, 23, 1788-1791.
5. R. J. T. Houk, B. W. Jacobs, F. E. Gabaly, N. N. Chang, A. A. Talin, D. D. Graham, S. D. House, I. M. Robertson and M. D. Allendorf, *Nano Lett.*, 2009, 9, 3413-3418.
6. L. Ai, H. Yue and J. Jiang, *Journal of Materials Chemistry*, 2012, 22, 23447-23453.
7. L. S. Nair and C. T. Laurencin, *Journal of Biomedical Nanotechnology*, 2007, 3, 301-316.
8. G. De Cremer, B. F. Sels, J.-i. Hotta, M. B. J. Roeffaers, E. Bartholomeeusen, E. Coutiño-Gonzalez, V. Valtchev, D. E. De Vos, T. Vosch and J. Hofkens, *Advanced Materials*, 2010, 22, 957-960.
9. M. Choi, Z. Wu and E. Iglesia, *Journal of the American Chemical Society*, 2010, 132, 9129-9137.
10. K. E. deKrafft, C. Wang and W. Lin, *Advanced Materials*, 2012, 24, 2014-2018.
11. X. Huang, Z. Zeng, Z. Fan, J. Liu and H. Zhang, *Advanced Materials*, 2012, 24, 5979-6004.
12. H. Li, L. Han, J. Cooper-White and I. Kim, *Green Chemistry*, 2012, 14, 586-591.
13. L. You, Y. Mao and J. Ge, *The Journal of Physical Chemistry C*, 2012, 116, 10753-10759.
14. Z. Jin, M. Xiao, Z. Bao, P. Wang and J. Wang, *Angewandte Chemie International Edition*, 2012, 51, 6406-6410.
15. N. Stock and S. Biswas, *Chemical Reviews*, 2011, 112, 933-969.
16. K. M. Thomas, *Dalton Transactions*, 2009, 1487-1505.
17. P. Horcajada, C. Serre, D. Grosso, C. Boissière, S. Perruchas, C. Sanchez and G. Férey, *Advanced Materials*, 2009, 21, 1931-1935.
18. A. Dhakshinamoorthy, M. Alvaro, A. Corma and H. Garcia, *Dalton Transactions*, 2011, 40, 6344-6360.
19. G. Lu, O. K. Farha, W. Zhang, F. Huo and J. T. Hupp, *Advanced Materials*, 2012, 24, 3970-3974.
20. H.-L. Jiang, B. Liu, T. Akita, M. Haruta, H. Sakurai and Q. Xu, *Journal of the American Chemical Society*, 2009, 131, 11302-11303.
21. S. Hermes, M.-K. Schröter, R. Schmid, L. Khodeir, M. Muhler, A. Tissler, R. W. Fischer and R. A. Fischer, *Angewandte Chemie International Edition*, 2005, 44, 6237-6241.
22. Z. Sun, G. Li, L. Liu and H.-o. Liu, *Catalysis Communications*, 2012, 27, 200-205.
23. H. Liu, Y. Li, H. Jiang, C. Vargas and R. Luque, *Chemical Communications*, 2012, 48, 8431-8433.
24. X. Gu, Z.-H. Lu, H.-L. Jiang, T. Akita and Q. Xu, *Journal of the American Chemical Society*, 2011, 133, 11822-11825.

25. T. Ishida, M. Nagaoka, T. Akita and M. Haruta, *Chemistry – A European Journal*, 2008, 14, 8456-8460.
26. A. Henglein and D. Meisel, *Langmuir*, 1998, 14, 7392-7396.
27. G. Lubkowski, J. Kuhnhenn, M. Suhrke, U. Weinand, I. Endler, F. Meibner and S. Richter, *Nuclear Science, IEEE Transactions on*, 2012, 59, 792-796.
28. L. F. Dumée, K. Sears, B. Marmiroli, H. Amenitsch, X. Duan, R. Lamb, D. Buso, C. Huynh, S. Hawkins, S. Kentish, M. Duke, S. Gray, P. Innocenzi, A. J. Hill and P. Falcaro, *Carbon*, 2013, 51, 430-434.
29. P. M. Schoenecker, C. G. Carson, H. Jasuja, C. J. J. Flemming and K. S. Walton, *Industrial & Engineering Chemistry Research*, 2012, 51, 6513-6519.
30. S. S.-Y. Chui, S. M.-F. Lo, J. P. H. Charmant, A. G. Orpen and I. D. Williams, *Science*, 1999, 283, 1148-1150.
31. G. Majano and J. Pérez-Ramírez, *Advanced Materials*, 2013, 25, 1052-1057.
32. A. S. f. T. a. M. A. International, *Annual Book of ASTM Standards, ISO/ASTM 51205*, 2009.
33. K. Tan, N. Nijem, P. Canepa, Q. Gong, J. Li, T. Thonhauser and Y. J. Chabal, *Chemistry of Materials*, 2012, 24, 3153-3167.
34. J. B. DeCoste, G. W. Peterson, H. Jasuja, T. G. Glover, Y.-g. Huang and K. S. Walton, *Journal of Materials Chemistry A*, 2013, 1, 5642-5650.
35. F. Wang, H. Guo, Y. Chai, Y. Li and C. Liu, *Microporous and Mesoporous Materials*, 2013, 173, 181-188.
36. E. Borfecchia, S. Maurelli, D. Gianolio, E. Groppo, M. Chiesa, F. Bonino and C. Lamberti, *The Journal of Physical Chemistry C*, 2012, 116, 19839-19850.
37. H. R. Moon, J. H. Kim and M. P. Suh, *Angewandte Chemie International Edition*, 2005, 44, 1261-1265.
38. M. D. Allendorf, R. J. T. Houk, L. Andruszkiewicz, A. A. Talin, J. Pikarsky, A. Choudhury, K. A. Gall and P. J. Hesketh, *Journal of the American Chemical Society*, 2008, 130, 14404-14405.
39. C. Prestipino, L. Regli, J. G. Vitillo, F. Bonino, A. Damin, C. Lamberti, A. Zecchina, P. L. Solari, K. O. Kongshaug and S. Bordiga, *Chemistry of Materials*, 2006, 18, 1337-1346.
40. Z. Zhang, C. Shao, Y. Sun, J. Mu, M. Zhang, P. Zhang, Z. Guo, P. Liang, C. Wang and Y. Liu, *Journal of Materials Chemistry*, 2012, 22, 1387-1395.
41. Z. Li and H. C. Zeng, *Chemistry of Materials*, 2013, 25, 1761-1768.
42. A. Gangula, R. Podila, R. M, L. Karanam, C. Janardhana and A. M. Rao, *Langmuir*, 2011, 27, 15268-15274.
43. P. Zhang, C. Shao, Z. Zhang, M. Zhang, J. Mu, Z. Guo and Y. Liu, *Nanoscale*, 2011, 3, 3357-3363.

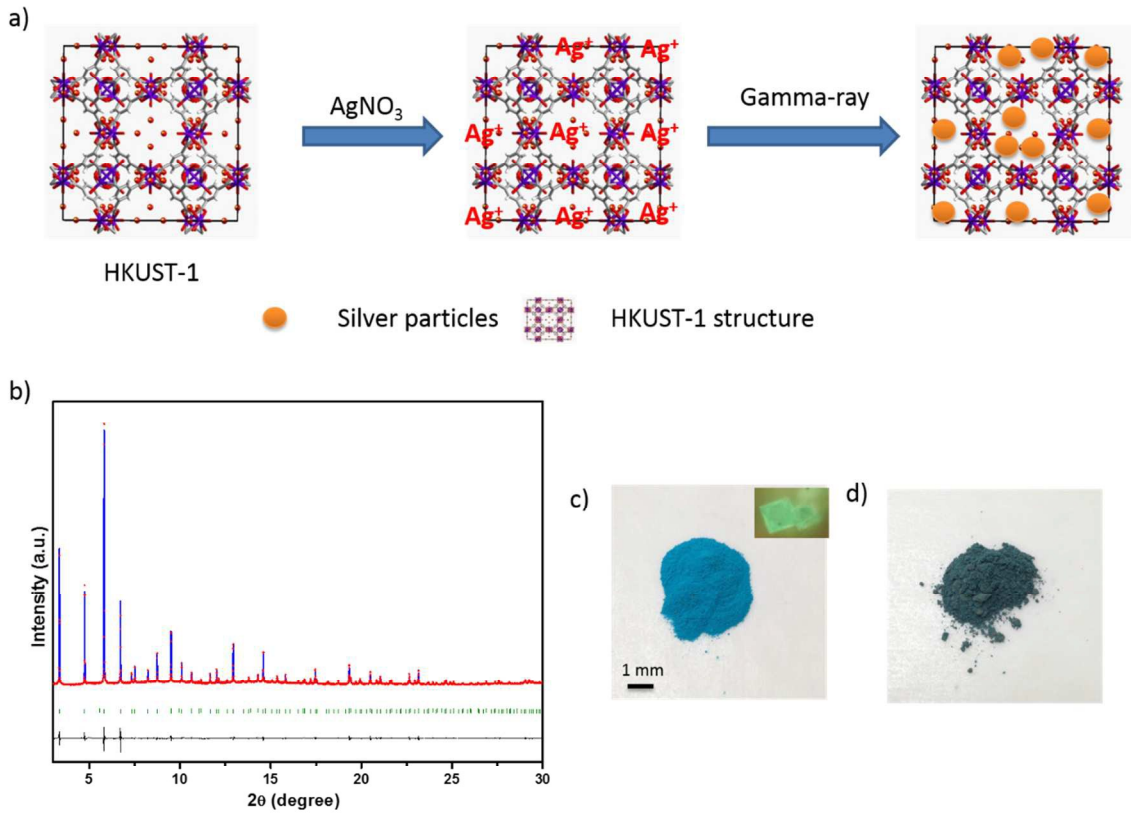

Figure 1 a) Schematic of Ag@HKUST-1 crystals preparation; b) Rietveld refinement results: the red cycle point indicates the calculated peak position, the blue line indicates the HKUST-1 powder samples peak position; Optical images of HKUST-1 crystals c) HKUST-1 d) 1 kGy Ag@HKUST-1

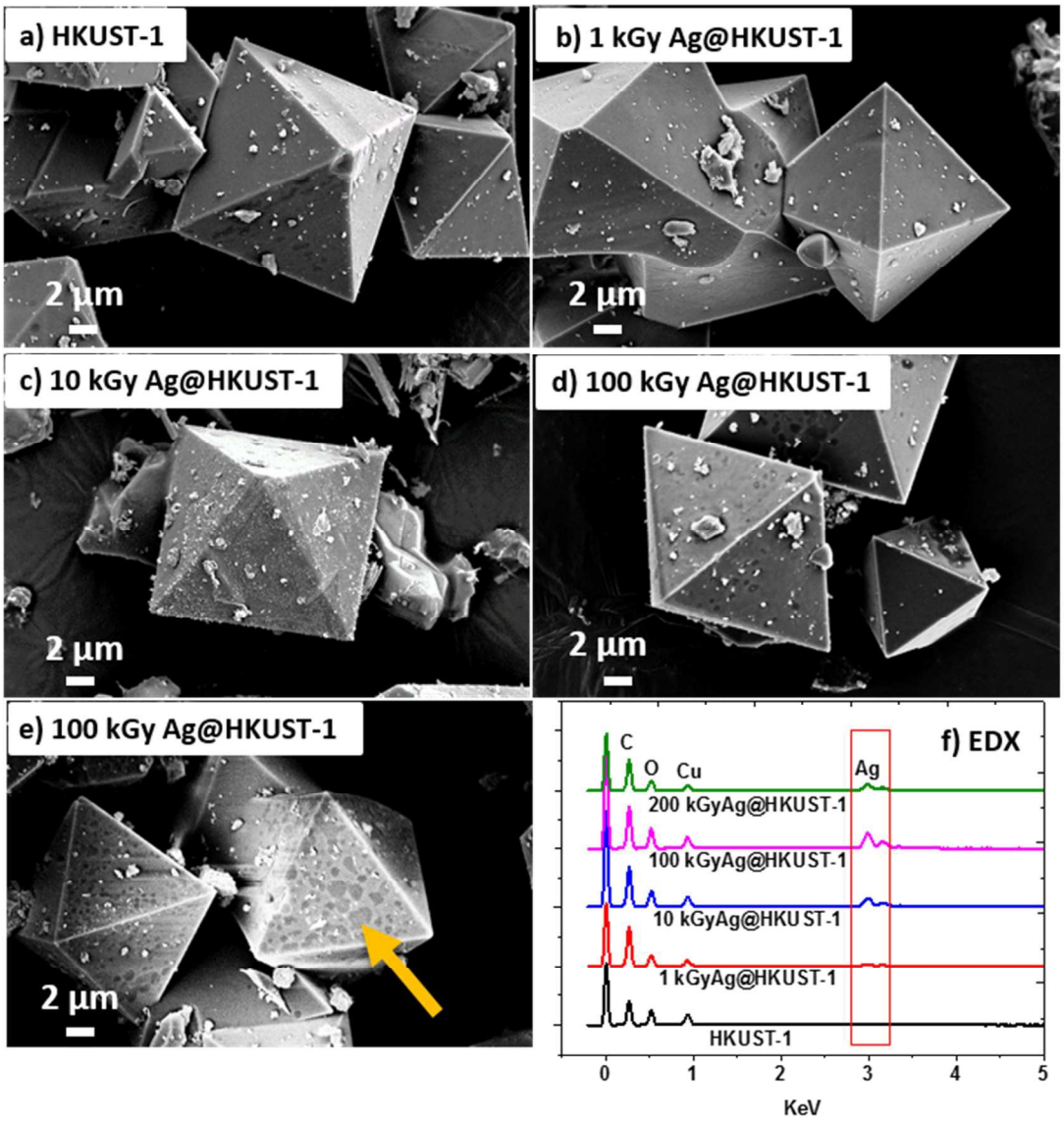

Figure 2 SEMs and EDX spectra of Ag@HKUST-1 crystals under different irradiation doses a) HKUST-1 b) 1 kGy c) 10 kGy d) 100 kGy e) 200 kGy f) EDX spectra

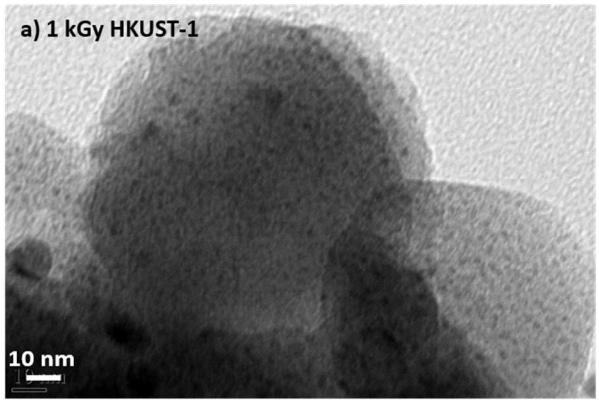

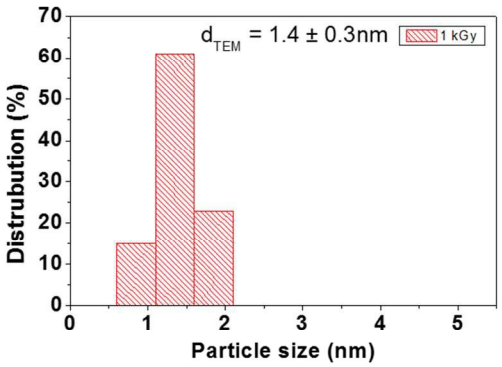

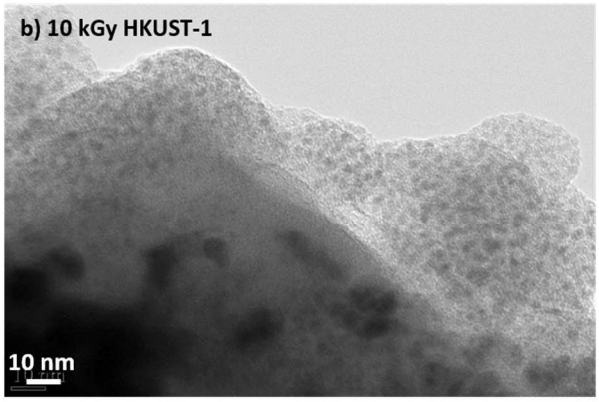

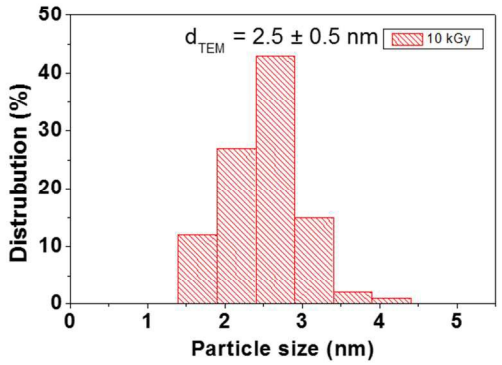

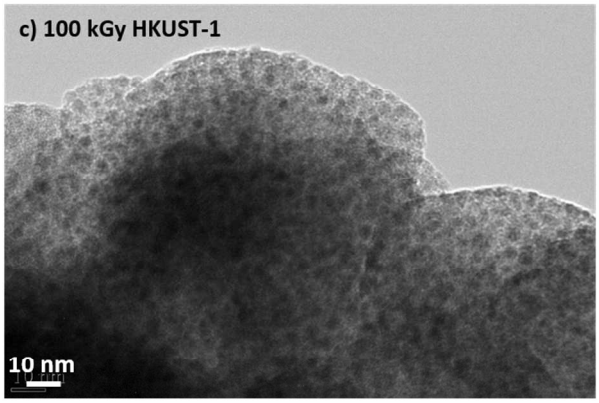

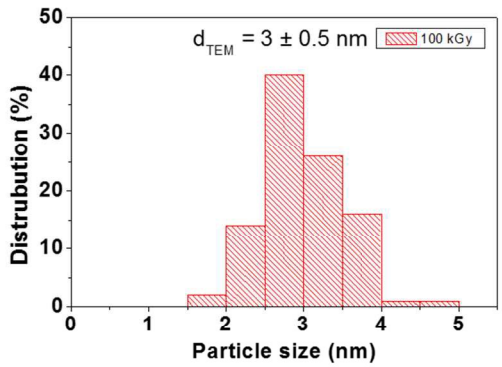

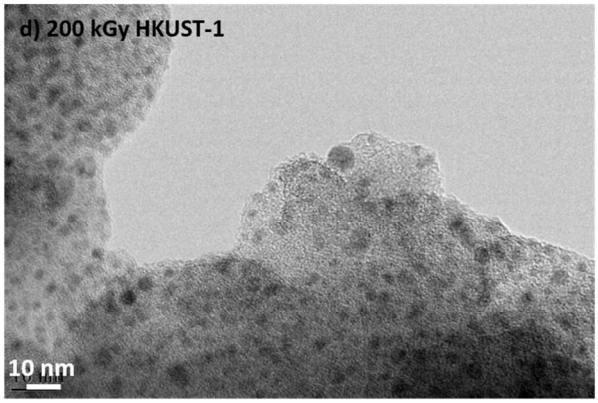

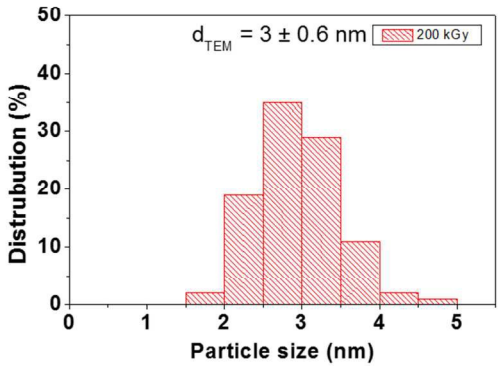

Figure 3 TEM images of Ag@HKUST-1 crystals and the corresponding size distribution histogram a) 1 kGy b) 10 kGy c) 100 kGy d) 200 kGy

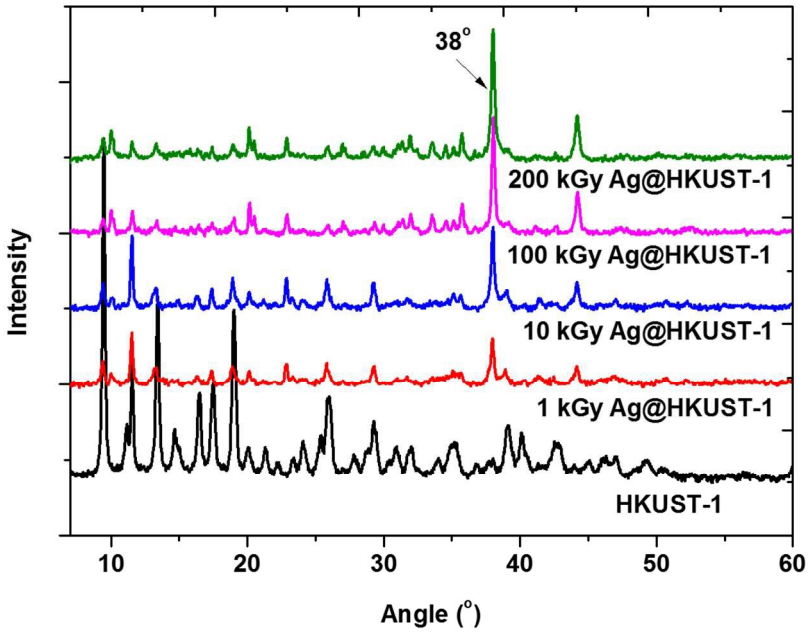

Figure 5 Powder x-ray diffraction patterns of Ag@HKUST-1 before and after different irradiation doses. The black arrow indicates the Ag (111) reflection centred at 2θ = 38°. HKUST-1 shows background reflections from the MOF which prevent observation of the Ag.

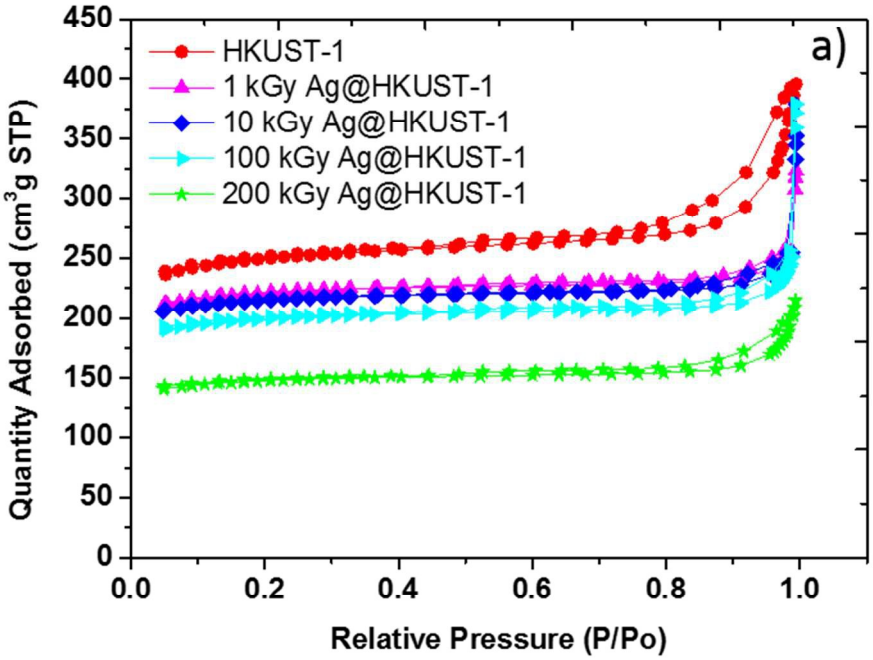

Figure 6 Nitrogen adsorption of Ag@HKUST-1 crystals (adsorption - desorption isotherms at 77 K)

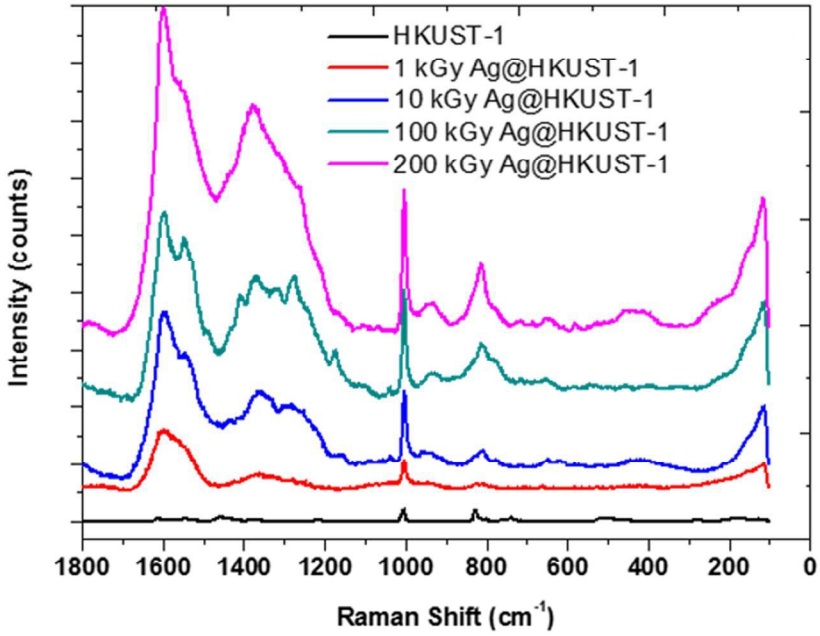

Figure 7 Raman spectra of Ag@HKUST-1 with a λ=514 nm: Ag@HKUST-1 with different gamma irradiation doses: HKUST-1 template (black line), 1 kGy Ag@HKUST-1 (red line), 10 kGy Ag@HKUST-1 (blue line), 100 kGy Ag@HKUST-1 (green line), 200 kGy Ag@HKUST-1 (pink line)

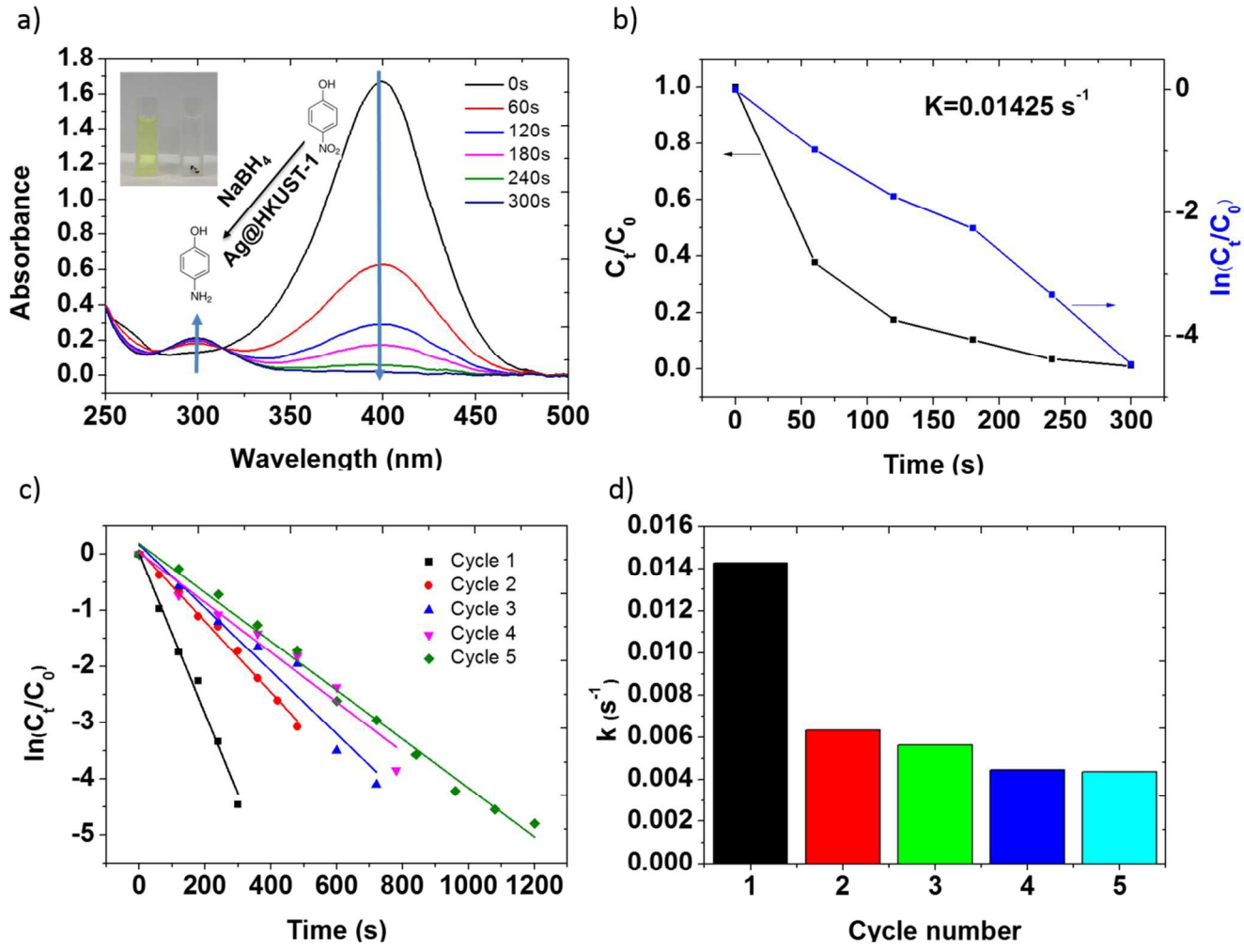

Figure 8 Reduction experiement of the 4-NP into 4-AP: (a) UV-vis absorption spectra successive UV-vis absorption spectra of the reduction of 4-NP by $NaBH_4$ in the presence of 100 kGy Ag@HKUST-1; (b) Plot of $\ln(C_t/C_0)$ against the reaction time; (c) Plot of $\ln(C_t/C_0)$ against the reaction time for five successive cycle reactions using 100 kGy Ag@HKUST-1 as catalyst;(d) The value of the rate constant k for each cycle with 100 kGy Ag@HKUST-1 as catalyst.

Table 1. Textural parameters and catalytic activities of Ag@HKUST-1 catalysts systems prepared from different irradiation dose for 4-NP reduction

Catalyst	Ag NPs average diameter(nm)	Surface area (m^2/g)	Ag used for catalyst (mg)	Ag NPs Loading (wt.%)[a]	k(10^{-3} s^{-1})	K_{Ag}(10-2 s^{-1} g^{-1})
1 kGy Ag@HKUST-1	1.4±0.7	650.62	2	3.77	14.46	19.17
10 kGy Ag@HKUST-1	2.5±1.6	633.39	2	8.35	13.53	8.10
100 kGy Ag@HKUST-1	3±1.8	588.34	2	9.33	14.25	7.63
200 kGy Ag@HKUST-1	3±3	436.61	2	10.66	11.71	5.49

[a] The value was determined by TGA